



Manufacturing and characterisations of hafnia-based materials for aerospace applications

Aurélie Julian-Jankowiak, Louise Sévin, Volatiana Razafindramanana, Lisa Audouard, Jean-François Justin, Pierre Bertrand, Cécile Langlade, Matthieu Garcia

► To cite this version:

Aurélie Julian-Jankowiak, Louise Sévin, Volatiana Razafindramanana, Lisa Audouard, Jean-François Justin, et al.. Manufacturing and characterisations of hafnia-based materials for aerospace applications. 9 EUROPEAN CONFERENCE FOR AERONAUTICS AND SPACE SCIENCES (EUCASS-3AF 2022, Jun 2022, Lille, France. 10.13009/EUCASS2022-6082 . hal-03773731

HAL Id: hal-03773731

<https://hal.science/hal-03773731>

Submitted on 9 Sep 2022

HAL is a multi-disciplinary open access archive for the deposit and dissemination of scientific research documents, whether they are published or not. The documents may come from teaching and research institutions in France or abroad, or from public or private research centers.

L'archive ouverte pluridisciplinaire **HAL**, est destinée au dépôt et à la diffusion de documents scientifiques de niveau recherche, publiés ou non, émanant des établissements d'enseignement et de recherche français ou étrangers, des laboratoires publics ou privés.

Manufacturing and characterisations of hafnia-based materials for aerospace applications

A. Julian-Jankowiak ^a, L. Sévin ^{abc}, V. Razafindramanana ^c, L. Audouard ^{abc}, J-F. Justin ^a, P. Bertrand ^b, C. Langlade ^b, M. Garcia ^c

^a ONERA/DMAS-Université de Paris-Saclay, Châtillon, 92320 France
(aurelie.jankowiak@onera.fr; louise.sevin@onera.fr; lisa.audouard@onera.fr; jean-francois.justin@onera.fr)

^b Université de Bourgogne Franche-Comté, laboratoire ICB UMR CNRS-UB-UTBM 6303, 90010 Belfort France
(cecile.langlade@utbm.fr; pierre.bertrand@utbm.fr)

^c Direction des systèmes orbitaux, CNES, Toulouse, 31410, France
(Matthieu.Garcia@cnes.fr)

Abstract

Considering more severe operating conditions in combustion chambers, new systems of materials are developed by CNES, ONERA and ICB. In the present study, stabilised hafnia has been chosen for the ceramic part of this system as its thermophysical properties are interesting compared to other ceramics. More precisely, hafnia based materials with different natures (Lu_2O_3 , Y_2O_3 and Gd_2O_3) and amounts of stabilisers have been manufactured using a solid state reaction. Fully stabilised materials were obtained and the microstructures and the thermal expansion coefficients up to 1550°C were investigated.

1. Introduction

Today, hydrazine is commonly used for space propulsion. However, the REACh regulation is threatening the use of this monopropellant, which is considered as “substance of very high concern” because of its high toxicity and might ban its use in a near future. In this regard, the need for new “green” propellant has become imperative for Europe to stay in the course of satellite propulsion. Thus, CNES and ONERA began to develop an alternative monopropellant with promising success in terms of energy efficiency and reduced toxicity. However these energetic compounds have the common points to develop harsh conditions which include a high temperature flame ($> 2700\text{ K}$) and very oxidising gases (particularly $\text{H}_2\text{O(g)}$). From there, CNES, ONERA and ICB-PMDM started research works focused on the development of new combustion chamber materials to answer previous needs.

This work is focused on the development of a 2700 K oxide resistant ceramic layer as Environmental Barrier Coating / Thermal Barrier Coating. The cubic-stabilized hafnia (HfO_2) seems to be one of the most promising candidates for thermal and environmental barriers applications in such conditions as it presents a high melting point, a low thermal conductivity and a relatively low thermal expansion compared to others ceramics oxides [1,2]. Only a few studies have been carried out on its high temperature thermo-structural properties and generally, with limited information up to 2273 K [3]. In the literature, studies are focused on partially stabilized zirconia based materials (PSZ), as it is used for Thermal Barrier Coatings in gas turbine engines. More recently papers deal with an ordered fluorite phase, the pyrochlore zirconia-based oxides [4,5]. However, in a combustion chamber submitted to higher temperatures, PSZ coatings will not fulfill anymore the requirements for a high reliability. In recent studies, hafnia appears to be a good candidate to be used as Environmental Barrier Coating [6] and also as Thermal Barrier Coating for thruster [7]. To reach phase stability up to 2700 K [8], the stabilization of the cubic phase is mandatory. Trivalent rare earth cations are commonly used to stabilize zirconia or hafnia. It was found that the ionic radius of the rare earth cation has a major impact on ceramics properties. Andrievskaya [9] and other authors [10] demonstrate that the melting point, the stability and the thermal expansion coefficient of the solid solution depend on the dopant rate and the ionic radius of the stabilizers.

In our previous studies, hafnia based samples with different doping strategies in terms of compositions have shown a high potential. In particular, high amounts of additives ($>33\text{ mol. \%}$) seem to be very promising [11,12].

To complete these results, hafnia samples with different additives as Lu_2O_3 , Y_2O_3 and Gd_2O_3 in the range of 14 mol. % to 50 mol. % are sintered using natural sintering. After that, the microstructure of the samples is investigated by Scanning Electron Microscopy to determine the grain size, homogeneity, porosity (rate and shape) and composition (by Electron Dispersive Spectroscopy) as these parameters are determinant for further characterisations. Finally, the

coefficient of thermal expansion (373-1773 K), is measured for each composition. Thus, the relationship between the microstructure, the composition and the thermal expansion as a function of the nature and the amount of rare earth oxide is established.

These results will be useful to complete our understanding on the influence of the additive on the stabilisation of hafnia.

2 Experimental procedure

Rare earth oxide (RE_2O_3) powders including gadolinium oxide, (purity>99.9%), yttrium oxide (purity>99.9%) and lutetium oxide (nanosized) were chosen as phase stabilizers for hafnium oxide (purity>99.9%). After drying overnight at 403 K, the powders were weighed to obtain 14, 20, 33, 40 and 50 mol. % rate of RE_2O_3 in HfO_2 .

The powder mixtures were ball-milled for 4 hours in ethanol using zirconia media and sieved (50 μm) after drying in a rotating evaporator. In the case of high RE_2O_3 concentrations (≥ 33 mol. %), the mixed powders were heat treated at 1823 K during 2 h in air in order to form the disordered cubic phase of the hafnia solid solution prior to the densification step to minimise the presence of defects such as porosities and composition inhomogeneities. Then, all the compositions were uniaxially pressed (20 mm in diameter) under a pressure of 50 MPa or pressed in a cold isostatic press under 700 MPa during 2 minutes. After that, they were sintered a first time at 2023 K for 6 h in air. A second thermal treatment was performed at 2273 K in an argon atmosphere in order to reach high densification levels and a similar microstructure between samples. Moreover, a re-oxidizing process (1173 K during 10h under air) was applied to the pellets to avoid any oxygen vacancies due to thermal treatment under reducing condition. All the materials and sintering conditions are listed Table 1.

The open porosities and apparent densities of these samples were measured by the Archimedes' method. Densification level was calculated as the ratio of the apparent density to the theoretical density obtained from X-ray diffractograms using MAUD or HighScore softwares and Rietveld or Pawley refinements.

For each sample, the identification of the phases was done using a Panalytical Empyrean X-ray diffractometer (Bragg-Brentano configuration, θ - θ and $\text{CuK}\alpha$ radiation) and MAUD or HighScore softwares. The diffraction range was from 10° to 110° with a 0.01° scanning step. Thus, lattice parameters were determined from XRD patterns to calculate the theoretical density of the materials using the Ingel and Lewis formula [11].

Microstructure examinations were performed by means of Scanning Electron Microscopy (SEM, Mira Tescan). The sample surfaces were prepared by polishing down to 0.25 μm . After a meticulous polishing of the surface (1/4 μm and vibrating polishing with a Colloidal Silica suspension), the average grain size was assessed by Electron BackScattered Diffraction (EBSD) with a SEM (Merlin, Zeiss).

The average linear Thermal Expansion Coefficient (TEC) was determined under air flow (20 mL/min) from 373 to 1823 K with a heating rate of 5 K/min using a high-temperature dilatometer (SETARAM, SETSYS Evolution) over one to three cycles of heating, depending on the composition. Parallelepipedic ceramic sample dimensions were approximately 5x5 mm² and 10 mm in length.

Table 1 : Theoretical density, apparent density and open porosity of the samples. (* from measured lattice parameters and the Ingel and Lewis formula)

RE_2O_3	RE_2O_3 content (mol. %)	Reference	Sintering conditions	Theoretical density* (g/cm ³)	Apparent density (g/cm ³)	Open porosity (%)
Y_2O_3	14	Y-14	2273K-2h	9.157	8.859	0.00
	20	Y-20	2273K-4h	8.657	8.402	0.00
	33	Y-33	2273K-4h	7.704	7.610	0.51
	40	Y-40	2273K-4h	7.240	7.104	0.31
	50	Y-50	2273K-4h	6.732	6.633	0.58
Lu_2O_3	14	Lu-14	2273K-2h	10.298	9.929	0.44
	20	Lu-20	2273K-4h	10.224	9.867	0.46
	33	Lu-33	2273K-4h	10.037	9.694	0.50
	40	Lu-40	2273K-2h	9.850	9.773	0.23
	50	Lu-50	2273K-2h	9.740	9.779	0.18
Gd_2O_3	14	Gd-14	2273K-2h	9.892	9.393	0.63
	40	Gd-40	2273K-2h	8.748	8.273	0.05

2 Results and discussion

2.1 Phase stabilization

The XRD patterns of the solid solutions of $\text{HfO}_2\text{-Y}_2\text{O}_3$, $\text{HfO}_2\text{-Lu}_2\text{O}_3$ and $\text{HfO}_2\text{-Gd}_2\text{O}_3$ as a function of the RE_2O_3 amount are presented in Figure 1. The XRD patterns of all samples can be indexed with Fm-3m space group cubic structure with published data of a non-doped HfO_2 ideal cubic phase (JCPDS n°00-053-0560) and a disordered cubic phase called fluorite of following composition $\text{Hf}_2\text{RE}_2\text{O}_7$ (JCPDS n°00-024-1406 for $\text{Hf}_2\text{Y}_2\text{O}_7$). Moreover, at concentration rate equal or higher than 33 mol. % of RE_2O_3 , the $\text{Hf}_2\text{RE}_2\text{O}_7$ phase should be considered for the analysis. This was already observed in our previous study [11,12]. For all patterns, neither the monoclinic phase nor the tetragonal phase are detected in the diagrams. Moreover, the formation of the pyrochlore-type phase is avoided as the empirical criteria $r_{\text{RE}3+}/r_{\text{Hf}4+} < 1.46$ is verified [13–15]. Indeed, in the case of the studied cations, this ratio is always lower than 1.26 and the conservation of the disordered cubic phase is confirmed.

For materials with Y_2O_3 and Gd_2O_3 no secondary phases were detected whatever the RE_2O_3 concentration. In the case of $\text{HfO}_2\text{-Lu}_2\text{O}_3$ materials, some characteristic peaks of the Lu_2O_3 phase are observed for the 50-Lu material as it can be seen in the Figure 1.

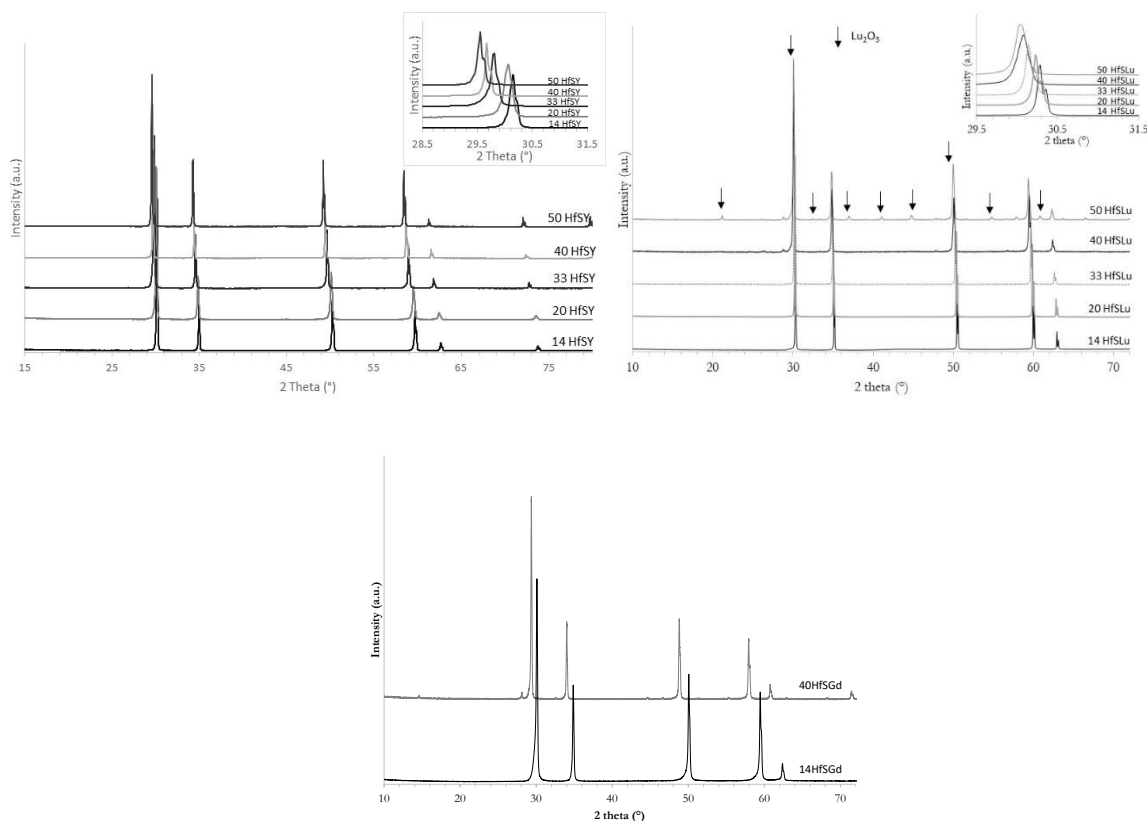


Figure 1 : XRD patterns of (a) $\text{HfO}_2\text{-}x$ mol. % Y_2O_3 ($x = 14, 20, 33, 40$ and 50), (b) $\text{HfO}_2\text{-}y$ mol. % Lu_2O_3 ($y = 14, 20, 33, 40$ and 50) and (c) $\text{HfO}_2\text{-}z$ mol. % Gd_2O_3 ($z = 14$ and 40).

In the case of 50-Lu, the quantification of Lu_2O_3 was performed using the Direct Derivation Quant Method of the software after the Pawley fit. This method provides information of the approximate proportions of the different phases. The XRD pattern fit is presented in the Figure 2 and the quality factor Rwp is very good (< 10) indicating the good refinement. Thus, the amount of Lu_2O_3 in this composition is around 23 w. %.

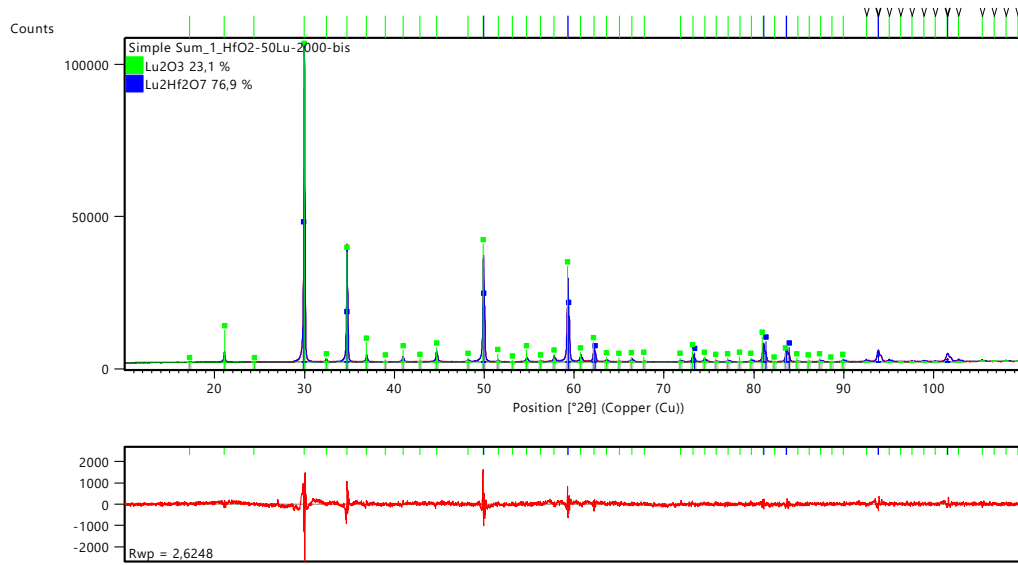


Figure 2 : Pawley refinement of the 50-Lu material.

Then, the lattice parameters of all materials were determined through Rietveld or Pawley refinements and their evolution as a function of the RE₂O₃ content is reported in the Figure 3.

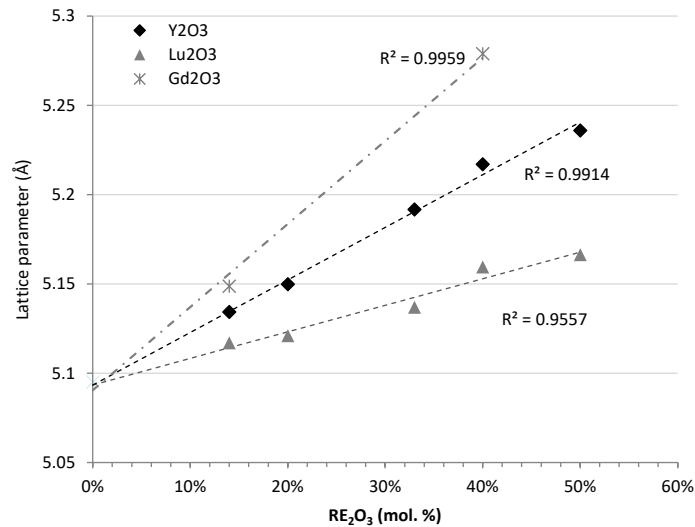


Figure 3 : Lattice parameters of the RE₂O₃-HfO₂ solid solution as a function of the RE₂O₃ content (RE= Gd, Y and Lu).

From the Figure 3, it can be noticed that for each RE₂O₃, the lattice parameter is linearly correlated to the RE₂O₃ amount in the solid solution, thus a Vegard's type law (Eq 1) is used to fit the data and good correlation rate (R²) are reached.

$$a = b \times x + c \quad (\text{Eq. 1})$$

Where a is the lattice parameter (Å), x the molar content of RE₂O₃ (%), b a constant depending on dopant species, and c the lattice parameter of the cubic hafnia without dopant (Å). Values for b and c for each RE₂O₃ studied in this paper are reported in the Table 2.

Table 2 : b and c values of the Vegard's law for the different rare earth oxides studied.

RE_2O_3	b (Å)	c (Å)
Gd_2O_3	$4.65 \cdot 10^{-1}$	5.0905
Y_2O_3	$2.94 \cdot 10^{-1}$	5.0934
Lu_2O_3	$1.49 \cdot 10^{-1}$	5.0934

From these results, the predicted lattice parameter for a pure cubic HfO_2 without any addition of RE_2O_3 by linear regression is close to 5.09 Å. This is perfectly correlated with the JCPD file for the cubic non-doped hafnia ($a=5.095$ Å) and other values from literature [16].

From these lattice parameters, the theoretical densities of the different compositions were calculated using the Ingel and Lewis formula [17] and the values are reported in the Table 1.

Regarding the lattice parameter for 14 and 40 mol. % of RE_2O_3 in the solid solution, it increases linearly with the ionic radius of RE^{3+} (Table 4) as it is shown in the Figure 4. Thus, a linear law (Eq. 2) can be used to fit the data.

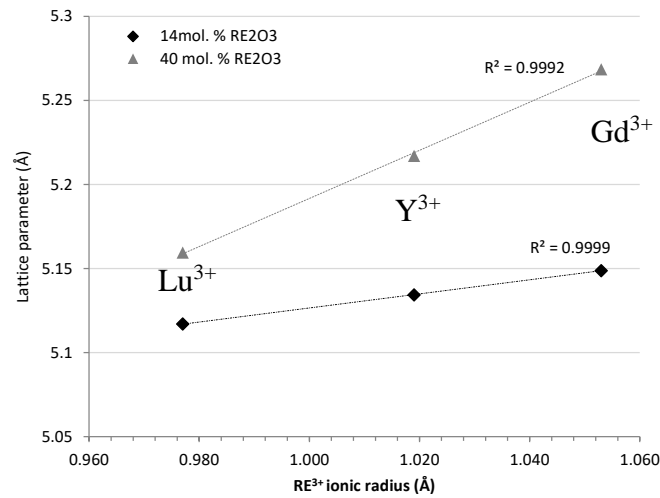


Figure 4 : Lattice parameters of the $\text{RE}_2\text{O}_3\text{-HfO}_2$ solid solution with 14 and 40 mol. % of RE_2O_3 ($\text{RE} = \text{Gd}, \text{Y}$ and Lu) as a function of the RE^{3+} ionic radius

$$a = d \times r_{\text{RE}^{3+}} + e \quad (\text{Eq. 2})$$

Where a is the lattice parameter (Å), r the ionic radius of the RE^{3+} ion (Å), d a constant depending on the species amount. Values for d and e for 14 and 40 mol. % of RE_2O_3 are summarized in the Table 2.

Table 3 : d and e values of the Eq 2.

Mol. % RE_2O_3	d	e (Å)
14	0.41817	4.708
40	1.431	3.760

Finally, it can be concluded that all the solid solutions can be obtained with the solid state reaction. The evolution of the lattice parameter is linear whatever the amount of RE_2O_3 and the higher the ionic radius of RE^{3+} cation, the higher the lattice parameter.

2.1 Microstructures

After XRD analyses, the microstructures were finely characterized to determine the porosity level, the grain size and the homogeneity of the materials. The densification levels are superior to 94 % of the theoretical density (Table 1), thus all the samples are considered as fully dense.

Regarding materials with Y_2O_3 , all the compositions are homogeneous until 33 mol. %, beyond this limit very small Y_2O_3 -rich regions are detected in SEM examinations (not shown) (Figure 5). As XRD analyses, do not detect these Y_2O_3 -rich areas, thus these regions are very limited and we conclude that all the solid solutions are fully formed with

an homogeneous composition. Moreover, the SEM examinations confirm the good densification level of the samples (Figure 5).

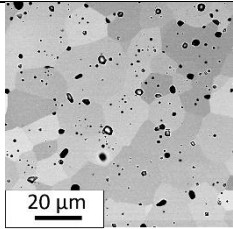
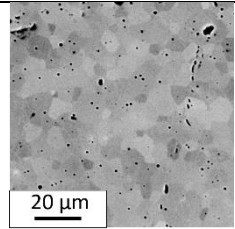
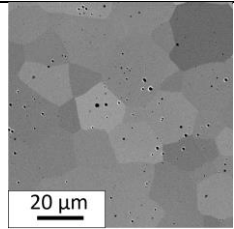
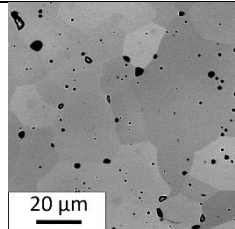
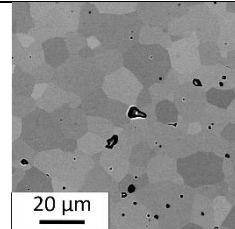
14 mol. % Y_2O_3	20 mol. % Y_2O_3	33 mol. % Y_2O_3	40 mol. % Y_2O_3	50 mol. % Y_2O_3
				
GS = 17.4 μm	GS = 15.6 μm	GS = 20.2 μm	GS = 20.2 μm	GS = 10.3 μm

Figure 5 : SEM examinations of HfO_2 - Y_2O_3 solid solution as a function of the RE_2O_3 amount. GS indicate the Grain Size determined through EBSD image analyses.

The grain size is assessed through EBSD cartographies (for 14, 20 and 33-Y) as this technique allows to take into account a large amount of grains. The software Orientation Imaging Microscopy Analysis™ was used to determine the grain size distribution in number. Several filters and hypotheses were applied such as exclusion of the grains at the edge of the picture and modelling of the grains as circles. For 40 and 50-Y samples the linear intercept method has been used.

All the materials exhibit an average grain size ranging from 10 to 20 μm , thus, the microstructures are considered equivalent.

The influence of the RE^{3+} cation of the microstructures is presented in Figure 6. Thus, for 14 mol. % of RE_2O_3 all the microstructures are homogeneous and equivalent with the same mean grain size. When the amount of RE_2O_3 reach 40 mol. % grain growth is observed for the solid solution with Lu_2O_3 .

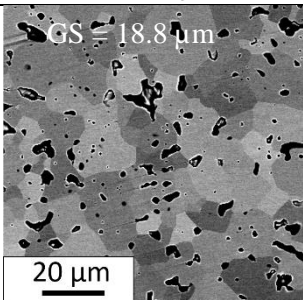
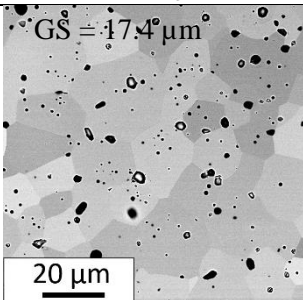
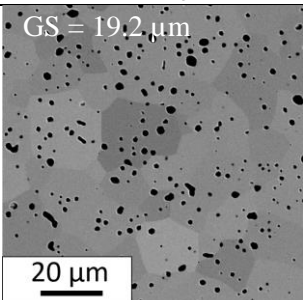
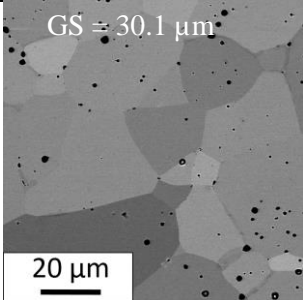
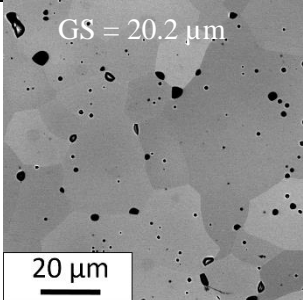
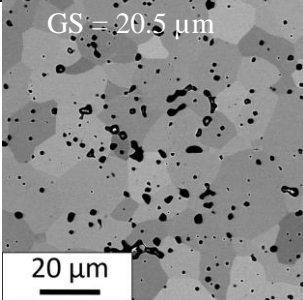
	Lu_2O_3	Y_2O_3	Gd_2O_3
14 mol. %	 GS = 18.8 μm	 GS = 17.4 μm	 GS = 19.2 μm
40 mol. %	 GS = 30.1 μm	 GS = 20.2 μm	 GS = 20.5 μm

Figure 6 : SEM examinations of HfO_2 - RE_2O_3 solid solution for 14 and 40 mol. % of RE_2O_3 ($RE = Gd, Y$ and Lu). GS indicate the Grain Size determined through EBSD image analyses.

To conclude, microstructures are equivalent with a mean grain size ranging from 12 to 20 μm whatever the amount of RE_2O_3 and the nature of RE^{3+} with a slight increase in the mean diameter to 30 μm for 40 mol. % of Lu_2O_3 .

2.1 Thermal expansion

Thermal expansion of the studied solid solutions is measured in air and the thermal expansion coefficient (TEC) is calculated as the slope between 373 and 1823 K.

Regarding solid solutions with Y_2O_3 (Figure 7), it can be noted that first the TEC decreases up to 40 mol. % of Y_2O_3 and then it increases again for 50 mol. % [12]. Thus, the lower TEC is reached for solid solutions with 40 mol. % of Y_2O_3 .

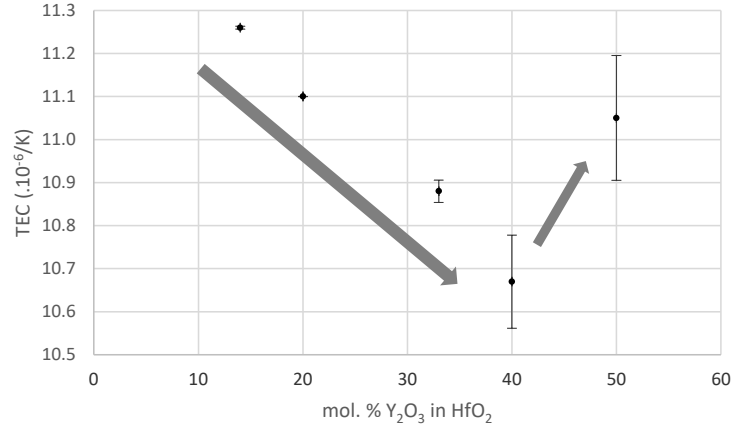


Figure 7 : Thermal expansion coefficient of HfO_2 - Y_2O_3 solid solutions as a function of the amount of Y_2O_3

Marrochelli et al. [18, 19] have studied the thermal expansion of non-stoichiometric oxides as solid solutions with fluorite structures similar to that presented in this paper and have proposed two phenomena to explain its variations: first the ionic radius of the RE^{3+} larger than Hf^{4+} and secondly the lattice relaxation around oxygen vacancies.

A lot of studies considered low content of RE_2O_3 (< 12 mol. %) compared to this study. Then, HfO_2 is mostly stabilized in the tetragonal phase and the authors often observed an increase in the TEC with the increase of the RE_2O_3 amount [20, 21]. In this paper, we study solid solution with higher amounts of RE_2O_3 and a decrease in the TEC is observed.

The Born-Landé equation (Eq. 3) considers the energy of the crystal lattice (U) which is inversely proportional to the dilatation.

$$U = \underbrace{\frac{N_A e^2}{4\pi\epsilon_0}}_{F1} M \underbrace{\left(1 - \frac{1}{n}\right)}_{F2} |Q^+||Q^-| \frac{1}{r_0} \propto \frac{1}{\alpha} \quad (\text{Eq. 3})$$

Where N_A is the Avogadro's number (mol^{-1}), e the charge of an electron (C), ϵ_0 the vacuum dielectric permittivity ($\text{C}^2/\text{J.m}$), M the Mandelung's constant, n the Born exponent, Q^+ and Q^- the number of cationic and anionic charges, r_0 the distance between ions (m) and α the thermal expansion coefficient (K^{-1}). Moreover, F1 is a constant and F2 is calculated to be 2.519 for fluorite structures.

When the amount of Y_2O_3 increases, Q^+ , Q^- and r_0 vary. Considering only Q^+ and Q^- , the TEC should increase with the amount of Y_2O_3 whereas the inverse is observed. Thus, r_0 seems to be the predominant factor governing the dilatation of the solid solution in the present case.

When increasing the amount of Y_2O_3 , the content of oxygen vacancies rises as expressed in Kröger-Vink notation (Eq. 4).



These oxygen vacancies imply electrostatic interactions..Marrochelli et al. have shown from experiments and simulations that removing an oxygen ion induces local distortions which lead to a contraction of the lattice as shown in Figure 8. The creation of an oxygen vacancy resulting from the remove of an oxygen ion modifies the electrostatic interactions and especially the repulsion of the cations. Thus, anions are attracted closer to the vacancy as there is no more oxygen ion close to it. Some authors have shown that electrostatic interactions may dominate around oxygen

vacancies unlike steric ones [22, 23]. Moreover, the vacancy radius due the oxygen vacancy is around 0.87 Å [19] which is largely lower than the oxygen ionic radius and the Re^{3+} radius (Table 4). This may explain the observed TEC decrease with the Y_2O_3 content.

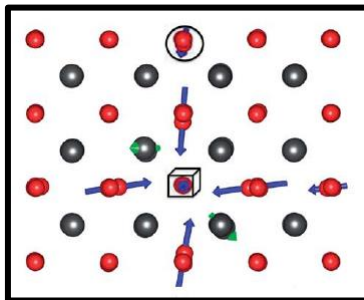


Figure 8 : Schematic view of the lattice contraction around oxygen vacancies

When the amount of Y_2O_3 becomes higher than 40 mol % a new increase in the TEC is observed and can be explained by the fact that the number of Y-O bonds becomes higher than the Hf-O bonds. As the binding energy of Y-O is lower than the Hf-O one (Table 4), thus increasing the amount of Y-O bonds leads to a global decrease of the lattice energy and thus an increase in the dilatation. Thus, the studies seem to indicate that the thermal expansion of the lattice is first increasing with the amount of stabilizer as the bond strengths become weaker (≤ 12 mol. %). However, above a certain amount of stabilizer (> 12 mol. %); a contraction of the lattice is observed as the more the amount of stabilizer, the more the amount of oxygen vacancies. Thus, these defects can reorganize in many ways, contracting the lattice. At very high amount of RE_2O_3 (> 40 mol. %) the dilatation increases again as RE-O bonds are numerous and weaker than Hf-O bonds.

Table 4 : Ionic radius, atomic weight and binding energy of studied ions.

	Hf^{4+}	Lu^{3+}	Y^{3+}	Gd^{3+}
Ionic radius (Å)	0.83	0.977	1.019	1.053
$\Delta H_{f(298)}(\text{RE-O})$ (kJ/mol)	791 ± 8	695 ± 13	715 ± 30	716 ± 7
Atomic weight (g/mol)	178.49	174.97	88.91	157.30

Regarding the influence of the ionic radius on the thermal expansion, the TEC of all the compositions are reported in Figure 9. For solid solutions with Gd_2O_3 and Lu_2O_3 the same evolution of the TEC than materials with Y_2O_3 is observed. Moreover, for 14 mol. % of RE_2O_3 , solid solution with Y_2O_3 exhibits the lower TEC. These results show that the TEC is not directly linked to the RE^{3+} ionic radius as it was already observed for compositions with Y_2O_3 .

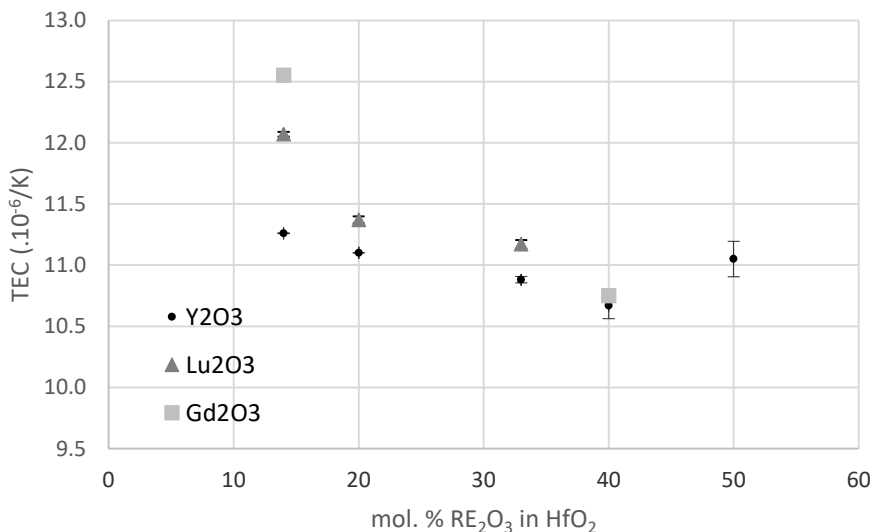


Figure 9 : Thermal expansion coefficients of $\text{HfO}_2\text{-RE}_2\text{O}_3$ solid solutions (RE= Gd, Y and Lu).

Considering only the influence of the ionic radius of RE^{3+} and a fixed amount of RE_2O_3 (14 mol.%), Q^+ and Q^- are equal for all the RE_2O_3 , thus, only r_0 varies. However, r_0 is not directly correlated to the RE^{3+} ionic radius, it depends also on the charge of the system. In the systems ZrO_2 -(Y-Yb-Gd) $_2O_3$ studied by Yashima et al. [23] the bond length is ranged as follow: $r(Y-O) < r(Yb-O) < r(Gd-O)$. Considering that HfO_2 and ZrO_2 have very similar electronic structures and that Yb and Lu are neighbors in the periodic table, we can consider this classification: $r(Y-O) < r(Lu-O) < r(Gd-O)$. This can explain the TEC evolution as a function of RE^{3+} . The short bond length between Y^{3+} and O^{2-} can explain the low TEC reached with Y_2O_3 compared to the other RE_2O_3 .

Comparing Y_2O_3 , Lu_2O_3 and Gd_2O_3 -based systems, the same trends are observed. Measurements for 40 and 50-Lu are in progress, however from the Figure 9 the TEC measured for 14-Lu, 20-Lu and 33-Lu are always slightly higher than the TEC for the same compositions with Y_2O_3 . The same observation can be done for 40-Gd and 40-Y compositions. The TEC of 40-Gd is still higher than the one of 40-Y, however, the difference between the two TECs is very small compared to compositions 14-Gd and 14-Y. Thus, it seems that the influence of the bond length RE-O decreases with the increase of the amount of Re_2O_3 in the solid solution. It is possible that the influence of the ionic radius of RE^{3+} becomes predominant over the bond length in the r_0 calculation.

3. Conclusions

This study is focused on the development of an ultra-high temperature ceramic coating for satellites combustion chambers. Thus, stabilized hafnia has been chosen for its appropriate thermophysical properties and the influence of different amounts and natures of stabilizers for hafnia have been studied. The desired cubic phase of stabilized hafnia has been obtained for all the compositions, which has been verified with XRD analysis. Moreover, the resulting microstructures are equivalent in terms of homogeneity, porosity and grain size. However, the ionic radius of the cation and its amount influence the lattice parameter, and thus the thermal expansion of the lattice. Indeed, the more the amount of stabilizer, the higher the lattice parameter and the more the amount of oxygen vacancies. This last point modifies the electronic interactions in the lattice and influences the thermal expansion. Between, 14 mol. % and 40 mol.% of RE_2O_3 , the thermal expansion coefficient decreases due to lattice contraction around the oxygen vacancies. Then, an increase is observed for Y_2O_3 stabiliser as Y-O bonds are weaker than Hf-O bonds.

4. References

- Haggerty, R. P., Sarin, P., Apostolov, Z. D., Driemeyer, P. E. & Kriven, W. M. Thermal Expansion of HfO_2 and ZrO_2 . *J. Am. Ceram. Soc.* **97**, 2213–2222 (2014).
- Stecura, S., Campbell, W. J., United States & Bureau of Mines. *Thermal expansion and phase inversion of rare-earth oxides*. (U.S. Department of the Interior, Bureau of Mines, 1961).
- Buckley, J. D. W. *Effects of Cyclic Heating and Thermal Shock on Hafnia Stabilized with Calcia, Magnesia, and Ytria*. <https://ntrs.nasa.gov/search.jsp?R=19690025169> (1969).
- Fergus, J. W. Zirconia and Pyrochlore Oxides for Thermal Barrier Coatings in Gas Turbine Engines. *Metall. Mater. Trans. E* **1**, 118–131 (2014).
- Extreme Temperature Coatings for Future Gas Turbine Engines. *ResearchGate* https://www.researchgate.net/publication/267504229_Extreme_Temperature_Coatings_for_Future_Gas_Turbine_Engines.
- Zhu, D. Advanced Environmental Barrier Coating Development for SiC/SiC Ceramic Matrix Composites: NASA's Perspectives. (2016).
- Zhu, D. *Hafnia-Based Materials Developed for Advanced Thermal/Environmental Barrier Coating Applications*. <https://ntrs.nasa.gov/search.jsp?R=20050192261> (2004).
- Wang, J., Li, H. P. & Stevens, R. Hafnia and hafnia-toughened ceramics. *J. Mater. Sci.* **27**, 5397–5430 (1992).
- Andrievskaya, E. R. Phase equilibria in the refractory oxide systems of zirconia, hafnia and yttria with rare-earth oxides. *J. Eur. Ceram. Soc.* **28**, 2363–2388 (2008).
- Duran, P. & Pascual, C. Phase equilibria and ordering in the system HfO_2 - Yb_2O_3 . *J. Mater. Sci.* **19**, 1178–1184 (1984).
- Sévin, L. et al. Effect of high-content Ytria on the thermal expansion behaviour and ionic conductivity of a stabilised cubic Hafnia. *J. Eur. Ceram. Soc.* **40**, 5859–5869 (2020).
- Sevin, L. Développement de matériaux Ultra-Haute Température : optimisation des propriétés thermomécaniques d'un composite à gradient de propriétés. (Bourgogne Franche-Comté, 2021).
- Karthik, C., Anderson, T. J., Gout, D. & Ubic, R. Transmission electron microscopic study of pyrochlore to defect-fluorite transition in rare-earth pyrohafnates. *J. Solid State Chem.* **194**, 168–172 (2012).

14. Subramanian, M. A., Aravamudan, G. & Subba Rao, G. V. Oxide pyrochlores — A review. *Prog. Solid State Chem.* **15**, 55–143 (1983).
15. Popov, V. V. *et al.* Fluorite-pyrochlore phase transition in nanostructured $\text{Ln}_2\text{Hf}_2\text{O}_7$ ($\text{Ln} = \text{La-Lu}$). *J. Alloys Compd.* **689**, 669–679 (2016).
16. Stacy, D. W. & Wilder, D. R. The Yttria-Hafnia System. *J. Am. Ceram. Soc.* **58**, 285–288 (1975).
17. Ingel, R. P. & Iii, D. L. Lattice Parameters and Density for Y_2O_3 -Stabilized ZrO_2 . *J. Am. Ceram. Soc.* **69**, 325–332 (1986).
18. Marrocchelli, D., Bishop, S. R., Tuller, H. L. & Yildiz, B. Understanding Chemical Expansion in Non-Stoichiometric Oxides: Ceria and Zirconia Case Studies. *Adv. Funct. Mater.* **22**, 1958–1965 (2012).
19. Marrocchelli, D., Bishop, S. R. & Kilner, J. Chemical expansion and its dependence on the host cation radius. *J. Mater. Chem. A* **1**, 7673–7680 (2013).
20. Sameshima, S., Kawaminami, M. & Hirata, Y. Thermal Expansion of Rare-Earth-Doped Ceria Ceramics. *J. Ceram. Soc. Jpn.* **110**, 597–600 (2002).
21. Li, C. *et al.* Effect of Y doping on microstructure and thermophysical properties of yttria stabilized hafnia ceramics. *Ceram. Int.* **44**, 18213–18221 (2018).
22. Meyer, M., Nicoloso, N. & Jaenisch, V. Percolation model for the anomalous conductivity of fluorite-related oxides. *Phys. Rev. B* **56**, 5961–5966 (1997).
23. Yashima, M., Ishizawa, N. & Yoshimura, M. Application of an Ion-Packing Model Based on Defect Clusters to Zirconia Solid Solutions: I, Modeling and Local Structure of Solid Solutions. *J. Am. Ceram. Soc.* **75**, 1541–1549 (1992).